Investigating a Back Door Mechanism of Actin Phosphate Release by Steered Molecular Dynamics

Willy Wriggers* and Klaus Schulten
Department of Physics and Beckman Institute, University of Illinois at Urbana-Champaign, Urbana, Illinois

ABSTRACT In actin-based cell motility, phosphate (P_i) release after ATP hydrolysis is an essential biochemical process, but the actual pathway of P_i separation from actin is not well understood. We report a series of molecular dynamics simulations that induce the dissociation of P_i from actin. After cleavage from ATP, the singly protonated phosphate (HPO_4^{2-}) rotates about the ADP-associated Ca^{2+} ion, turning away from the negatively charged ADP towards the putative exit near His73. To reveal the microscopic processes underlying the release of P_i, adhesion forces were measured when pulling the substrate out of its binding pocket. The results suggest that the separation from the divalent cation is the rate-limiting step in P_i release. Protonation of HPO_4^{2-} to $H_2PO_4^{-}$ lowers the electrostatic barrier during P_i liberation from the ion. The simulations revealed a propensity of charged His73$^+$ to form a salt bridge with HPO_4^{2-}, but not with $H_2PO_4^{-}$. His73 stabilizes HPO_4^{2-} and, thereby, inhibits rapid P_i release from actin. Arg177 remains attached to P_i along the putative back door pathway, suggesting a shuttle function that facilitates the transport of P_i to a binding site on the protein surface. Proteins 1999;35:262–273. © 1999 Wiley-Liss, Inc.

Key words: actin function; ATP hydrolysis; divalent cation; phosphate titration; non-equilibrium molecular dynamics

INTRODUCTION

Actin filaments are dynamic polymers, whose time-dependent self-assembly in the cell cytoplasm plays an important role in processes involving cell motility.[1–3] ATP hydrolysis occurs on the actin subunits following their endwise addition to the elongating aggregate. The hydrolysis reaction[4] proceeds in two consecutive steps: (1) cleavage of the β-γ phosphoester bond of ATP (rate at 20°C: 0.035 s^{-1})[5]; (2) slow (0.0026 s^{-1})[5] liberation of the inorganic phosphate (P_i) from the protein. ATP is not required for actin polymerization, although ADP-bound filaments are less rigid and less stable than ATP-bound filaments.[6–8] Kinetic studies suggest that actin's ATPase activity serves as a destabilizing reaction that promotes depolymerization of the resulting ADP-bound filament.[7] It has been shown that P_i release, rather than phosphoester bond cleavage, is the crucial modifier of actin filament dynamics.[9]

Our work is concerned with the release of P_i into the medium after cleavage of the β-γ phosphoester bond. The coupling between ATP hydrolysis and filament elongation has been the subject of intense research (reviewed in Carlier[6]), but the basic structural mechanism of the chemical reaction still remains unknown. Crystal structures of monomeric actin in the ADP- and ATP-bound states[10] do not reveal any significant nucleotide-specific structural differences or residues that could enhance or regulate catalysis of the hydrolysis reaction.[11] The β- and γ-phosphates of ATP coordinate a Ca^{2+} ion in the gelsolin-actin crystal structure,[12] which is probably replaced by Mg^{2+} in the cell. As observed in other metalloenzymes such as DNA polymerase I,[13] the ion may play a crucial role in phosphoester bond hydrolysis.[14]

Earlier studies[15] have identified two pathways of diffusing water molecules that connect actin's enzymatic site with the solvent. The first diffusion pathway extends from the phosphate tail of the bound nucleotide to the prominent opening of the nucleotide binding pocket on the front face of the protein (Fig. 1a,b), where the adenine is exposed to the solvent. The second water diffusion pathway is oriented in the opposite direction and forms a distinct, alternative entrance for water molecules from the surrounding medium to access the enzymatic site. Figure 1c shows the corresponding small opening at His73 in the actin structure on the back face of the protein, through which P_i is visible. It was argued that the "front door" diffusion pathway facilitates the exchange of the nucleotide, whereas the distinct "back door" pathway (Fig. 1c) facilitates the release of P_i into the medium.[15]

Conventional molecular dynamics (MD) is considered to establish thermodynamic equilibrium in a simulated system.[16] Here, MD was used to investigate the fast relaxation of P_i after the ATP phosphoester bond cleavage (a perturbation of the system from equilibrium). To investigate the stability of the P_i binding pocket and to reveal the microscopic processes underlying the dissociation of P_i, we employed steered molecular dynamics (SMD) simulations

---

Fig. 1.   Putative pathway of P$_i$ release in actin. **a:** Front view; **b:** side view; **c:** back view. The protein in c is rotated relative to a by 180° about the horizontal axis and by 45° about the vertical axis, rotating subdomains 2 and 4 into the page. ADP (yellow), Ca^{2+} ion (orange), and P$_i$ (red) are shown in van-der-Waals representation. The protein (all residues except His73: blue) from the crystal structure of the actin:gelsolin segment-1 complex[12] is represented as a tube (a,b) and in van-der-Waals representation (c). Missing residues in the crystal structure were added as described in Methods. His73 (green) is shown in licorice style (a,b) and in van-der-Waals representation (c). The numbers identify actin's four structural subdomains.[10] The figure was generated using the molecular graphics program VMD.[47]

that dissociate P$_i$ from actin through the back door pathway. In SMD,[17,18] time-dependent external forces are applied to a ligand to induce its separation from a protein. SMD has proven to be successful in studies of the dissociation of the avidin-biotin complex[17,18] and the separation of retinal from bacteriorhodopsin.[19] The analysis of the interactions of the dissociating ligand with the binding pocket, as well as the recording of applied forces and of the ligand position, yield important structural information about ligand binding and unbinding.[20]

Simulations were carried out with either singly or doubly protonated P$_i$. In solution at neutral pH, both protonation states, HPO$_4^{2-}$ and H$_2$PO$_4^-$ (pKa = 7.21), exist. In the enzyme, after cleavage of the β-γ phosphoester bond by an in-line attack of a nucleophilic water molecule, P$_i$ is at first singly protonated.[21,22] Kinetic experiments suggest that subsequent titration of P$_i$ is required to allow release from actin.[9,23] In the living cell, the regulation of P$_i$ release by its protonation state is believed to act as a clock, altering in a time-dependent manner the stability and mechanical properties of the filament.[23]

Earlier studies singled out actin's methylated His73 as a putative modifier of P$_i$ release.[15] In the F-actin filament structure,[24] the toxin phalloidin binds to His73 near the entrance of the back door pathway (Fig. 1c) and, thereby, would delay P$_i$ release, as observed experimentally.[25] The histidine is methylated in all actin species except in *Naegleria gruberi.*[26] This remarkable methylation has puzzled researchers for 30 years (reviewed in Solomon and Rubenstein[27]), and the function of the methylation is still unknown. The model of P$_i$ release proposed in this work sheds new light on the role of the methylation of His73. One effect of the methylation of histidine is to shift the pKa of the imidazole on histidine. The pKa of histidine is 6.04 and that of 3-methylhistidine is 6.56.[28] Thus, at pH 7.0, methylhistidine will be considerably more charged than will be histidine. We investigated the effect of the P$_i$ protonation state on the behavior of charged His73 during the simulated release of the phosphate.

METHODS

Molecular dynamics simulations of actin were carried out using the program *X-PLOR*[29] with the *CHARMM22* all-hydrogen force field.[30] The structure of ATP-actin taken as the initial model was from the actin-gelsolin segment-1 complex.[12] Residues 40–50, missing in the crystal structure, were added based on coordinates from an earlier simulated structure of the protein (500 ps snapshot of trajectory CTC, described in Wriggers and Schulten[15]).

We obtained coordinates for 30 water molecules in the actin crystal structure[12] from Paul McLaughlin. Water molecules were placed when a peak in the crystallographic electron density had at least two hydrogen bonding partners within 2.8–3.5 Å distance (Paul McLaughlin, personal communication). This conservative restriction was necessary to confidently assign water binding sites at 2.5 Å resolution. We searched for additional buried water binding sites in actin with the program *Dowser.*[31] Only two additional water binding sites were found,[32] indicating that the crystal water molecules fill most of the buried cavities in the protein. Twelve of the crystal water molecules coordinate the charged phosphates and the Ca^{2+} ion in the enzymatic pocket,[32] consistent with earlier suggestions.[15] To account for the effect of surface water, the system was immersed in a water shell of 5.6 Å thickness, which corresponds to approximately two layers of water

molecules. The TIP3P water model[33] was used, although it was modified by omitting internal geometry constraints to provide water flexibility, as described elsewhere.[34] After solvation, the system included 1,159 water molecules and its size was 9,360 atoms.

The system was then prepared for P_i separation by cleavage of the O_β-P_γ bond of ATP: the three unprotonated oxygen atoms of P_i in the protonation state HPO_4^{2-} were superimposed with the three γ-oxygen atoms of ATP so that P_i was oriented with the hydroxyl facing the side opposed to the cleaved O_β-P_γ bond. After the placement of P_i, the γ-phosphate of ATP was deleted. This procedure approximated the structure immediately after attack of a nucleophilic water molecule with inversion of symmetry at the phosphate.[21,22]

Partial charges for ADP, HPO_4^{2-}, and $H_2PO_4^-$ atoms were calculated by means of the program *Gaussian,*[35] version 94, as described elsewhere.[32] The distances between the four phosphate oxygens of P_i were constrained[32] by an additional Hookean potential to 2.46 Å (distance derived from the geometry of ADP β-phosphate). The force constant used to preserve the tetrahedral geometry of P_i was 20 kcal mol^{-1} Å^{-2}.

The MD simulations were carried out on a cluster of Hewlett-Packard (Palo Alto, CA) 735/125 work-stations, using a 12 Å-cutoff, all-hydrogen force field, 1 fs integration step, and a dielectric constant ϵ = 1. The ADP · P_i-actin model was refined by minimization of the total energy. The system was assigned initial velocities according to a Maxwell distribution, heated up to 310 K in steps of 30 K in a 5-ps time period, and equilibrated at 310 K for 5 ps.

For the simulation, the protonation degrees of the histidine residues of actin were estimated based on their stability[15]; the side chain of His73 was simulated in the protonated (charged) state because of the stabilization of this state by the methyl group. Standard partial charges for the unmethylated histidines were provided by the *CHARMM*22 force field.[30] Charges for charged 3-methyl-histidine were combined from standard charges of an N-methylamide C-terminus and from charges of doubly protonated histidine in the standard force field, as described elsewhere.[32]

The extraction of P_i from actin was performed by application of external forces to the P_i phosphorus atom. These forces were implemented by restraining the phosphorus harmonically to a restraint point and by moving the restraint point with a constant velocity v in the desired direction. The most probable separation pathway was determined by inspection of the back face of the protein (Fig. 1c). The pull direction corresponds to the vector (0.250, 0.534, 0.807) in the coordinate system of PDB entry 1ATN.[10]† The force exerted on P_i is then

$$F = kd, \tag{1}$$

where k is the force constant, and d is the distance between the phosphorus atom and the restraint point. We chose k = $10k_B T$/Å,[2] where k_B is Boltzmann's constant and T is the temperature, and velocities v ranging from 0.0625 Å/ps to 1 Å/ps. These values of the force constant and the velocities correspond to a stiff spring in the drift regime[36,18] and allow spatial fluctuations of the phosphate of magnitude $\delta x = \sqrt{k_B T/k}$ = 0.32 Å. To realize a movement of the restraint point with nearly constant velocity, the position of the restraint point was changed every 100 fs by a distance of $v \times$ (100 fs) in the desired direction, following Isralewitz et al.[19] The α-carbons of actin's residues 31, 26, 56, 215, 307, and 333 at the front face of the protein (Fig. 1a) were held fixed to anchor actin during the forced separation of P_i.

The release of P_i in the presence of the Ca^{2+} ion was performed in simulations of length 20 ps using a velocity v = 0.75 Å/ps. The dissociation of P_i in the presence of the Ca^{2+} ion was simulated for various velocities v = 1, 0.5, 0.25, 0.125, and 0.0625 Å/ps in calculations of length 16, 32, 64, 128, and 256 ps, respectively. The simulations were carried out for both singly and doubly protonated phosphate. In the cases involving doubly protonated P_i, the phosphate was protonated after equilibration of the HPO_4^{2-} system. Divalent cation-free actin was simulated by replacing the Ca^{2+} ion with a water molecule.

RESULTS
β-γ Phosphoester Bond Cleavage

To prepare ATP-actin for the extraction of P_i, the β-γ phosphoester bond of ATP was cleaved as described in Methods. Figure 2 presents the resulting structure of ADP · P_i complexed with the Ca^{2+} ion after equilibration of the system. P_i is in the singly protonated state (HPO_4^{2-}) after cleavage of the β-γ bond.[21,22] Relative to its position in the ATP-actin crystal structure,[12] the phosphate rotated 70° about the Ca^{2+} ion. The ion itself moved 1.7 Å into the gap between P_i and the negatively charged β-phosphate of ADP. This displacement of P_i can be attributed to electrostatic repulsion away from the β-phosphate. A water molecule from the surrounding medium was hydrogen-bonded to both P_i and the β-phosphate, forming a bridge. After cleavage of the bond, P_i moved 3.4 Å in the direction of the putative back door exit (Fig. 1c), reducing the distance to the exit by 25%. A similar cleavage-related movement of P_i of 3.4 Å was observed in crystal structures of the ATPase fragment of the bovine 70-kDa heat shock cognate protein,[37] which is homologous to actin.[38]

Interactions With the Divalent Cation

The suggested separation path (Fig. 1c) provides the shortest route of P_i to the exterior of the protein. To test the viability of the path for dissociation, the phosphate was pulled along the path in various simulations described in Methods. Four stages of the dissociation process of P_i are shown in Figure 3. After the cleavage of the β-γ bond (t = 0 ps, Fig. 3a) and the initial heat-up and equilibration

†The actin coordinates used in this work[12] are not deposited in a structure database. PDB entry 1ATN corresponds to the actin-DNase 1 complex, in which actin adopts a similar conformation (backbone rms deviation 0.9 Å).
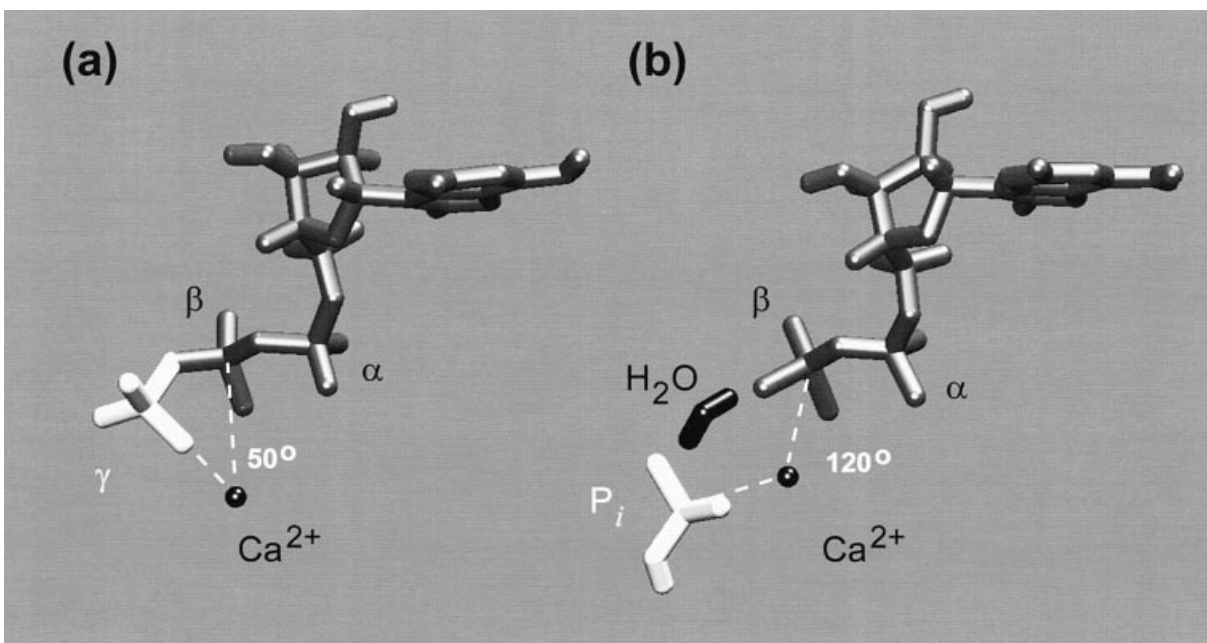
Fig. 2. Cleavage of the β-γ phosphoester bond of ATP. ADP (grey), the Ca^{2+} ion (black), a water molecule (black), and the γ-phosphate/P$_i$ (white) are shown in licorice representation. Also shown is the angle P$_β$-Ca^{2+}-P$_γ$. ATP is rotated by 180° about the vertical axis relative to its orientation in

Figure 1b. **a:** The structure of ATP in the initial crystal conformation[12]; **b:** the structure after 10 ps heat-up/equilibration at 310 K. HPO$_4^{2-}$ is oriented towards the back door exit (see Fig. 1c).

(t = 10 ps, Fig. 3b), the phosphate restraint point was moved until the exerted force was strong enough to pull the doubly protonated P$_i$ off the Ca^{2+} ion at t = 21.5 ps (Fig. 3c). At a displacement of 12 Å on the separation path, P$_i$ became exposed to the bulk solvent. At the end of the simulation, at t = 30 ps, the now exposed P$_i$ was displaced 13.5 Å from its position after equilibration (Fig. 3d).

The force applied to the phosphate along its path and its displacement after equilibration depends on the protonation state (Fig. 4a). Figure 4b shows the electrostatic energies governing interactions of the singly and doubly protonated phosphates with the Ca^{2+} ion. At first, the dissociation of the phosphates in the presence of the Ca^{2+} ion proceeds slowly: the phosphates remain tightly bound to the cation, while the applied forces are steadily increasing to values greater than 2,000 pN. In comparison, SMD simulations of the dissociation of the avidin-biotin complex[18] and the streptavidin-biotin complex[17] involved rupture forces lower than 800 pN. The rupture forces measured here are larger because of the strong electrostatic interaction of the phosphates with the Ca^{2+} ion (Fig. 4b). Eventually, the phosphate ruptures from the ion. This rupture event is manifested by a pronounced jump (6 Å) in the displacement caused by the relaxation of the harmonic restraints, and by a drop in the Ca^{2+} interaction energies. After the separation from the cation, forces exerted on the phosphates remain below 1,500 pN.

The protonation state of P$_i$ is a significant determinant of its behavior during dissociation. Release of HPO$_4^{2-}$ required a rupture force of 3,100 pN, whereas the liberation of H$_2$PO$_4^-$ involved a smaller rupture force of 2,400

pN. Protonation of P$_i$ lowered the electrostatic barrier ΔE for separation from the cation from ΔE = 440 kcal/mol (HPO$_4^{2-}$) to ΔE = 280 kcal/mol (H$_2$PO$_4^-$). We note that the Ca^{2+}—P$_i$ interaction energies given in Figure 4b represent unscreened electrostatic contributions that exclude the effects of the protein and solvent surrounding the phosphate. These interaction energies, which would arise in a medium of dielectric permittivity ϵ = 1 (e.g., in vacuo), are of the same order of magnitude as molar lattice energies of salt crystals.[39] The actual Ca^{2+}—P$_i$ interaction energies are expected to be considerably lower, as they scale with the inverse dielectric permittivity of the protein/solvent environment of the phosphate.[39] The exact dielectric properties of proteins are the subject of much debate; suggested values for the dielectric permittivity range from 10–36.[40,41] Assuming a low value ϵ = 15 for the sake of argument, we can estimate Ca^{2+}—P$_i$ interaction energies of ΔE = 29 kcal/mol (HPO$_4^{2-}$) and ΔE = 19 kcal/mol (H$_2$PO$_4^-$). We note that this simple estimate does not consider effects of ionic screening and the molecularity of the solvent medium. However, the continuum approach does predict trends surprisingly well in the experimentally observed interaction energies and solubilities of salt ions.[39]

The overall kinetics of ligand binding suggests that ligand dissociation occurs typically on a relatively fast, micro- to millisecond timescale,[42,43] even in cases where dissociation involves a diffusive motion of the ligand through the receptor protein.[42] What could be the rate-limiting step in actin's slow P$_i$ release (half-time for Ca^{2+}-actin ~500 s[44])? The estimated electrostatic barrier heights ΔE suggest that the slow release may be due to the
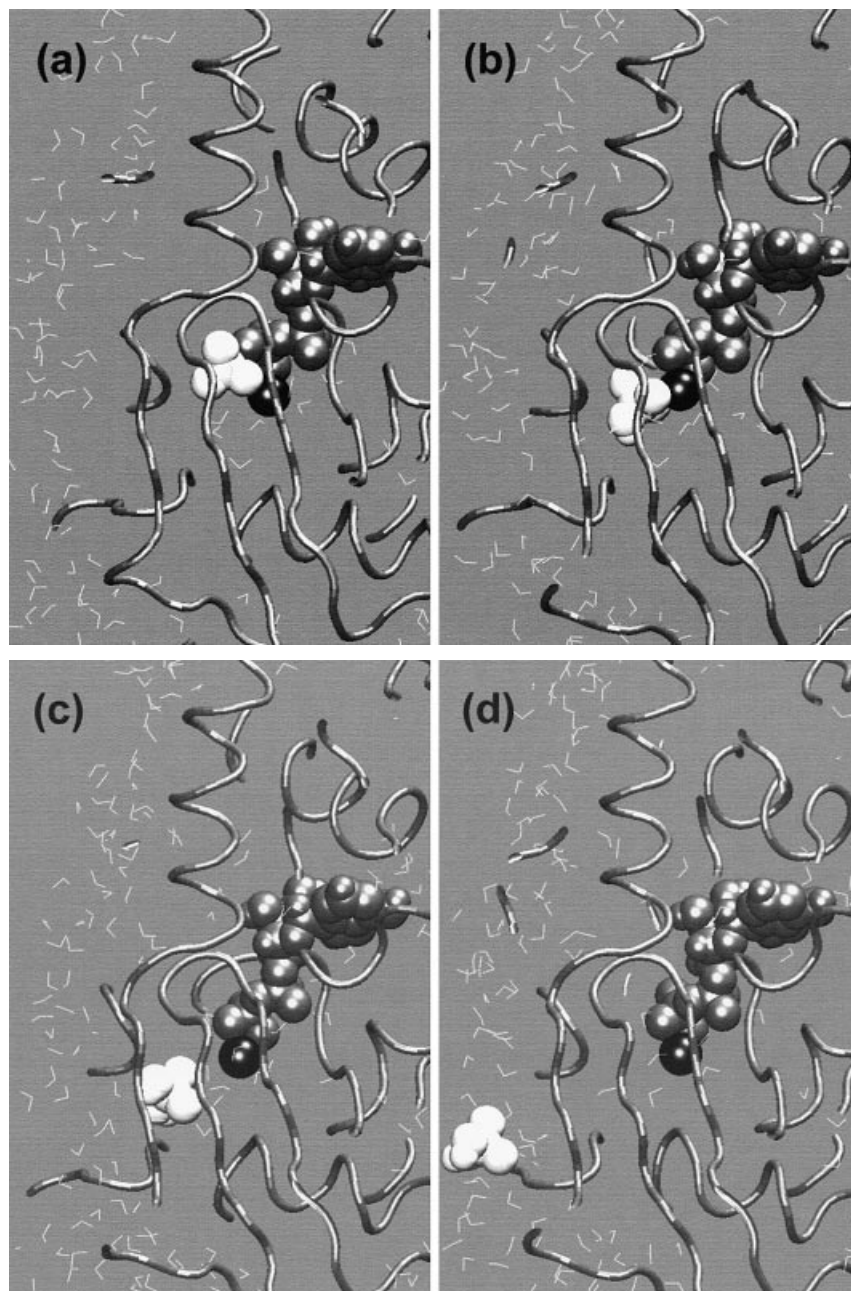
Fig. 3.   Actin's nucleotide vicinity at four stages of P_i release. The protein has been rotated by 180° about the vertical axis relative to its orientation in Figure 1b. ADP (grey), Ca^{2+} ion (black), and P_i (white) are shown in van-der-Waals sphere representation. The protein backbone is shown in tube representation. Water molecules surrounding the protein are shown in white line representation. **a:** $t = 0$ ps: cleavage of the ATP O_β-P_γ bond; **b:** $t = 10$ ps, start of the extraction of $H_2PO_4^-$; **c:** $t = 21.5$ ps, $H_2PO_4^-$ dissociates from the Ca^{2+} ion; **d:** $t = 30$ ps, end of the simulation. The figure was generated using the molecular graphics program VMD.[47]

strong Ca^{2+}—P_i interaction. According to Kramers/Arrhenius theory,[45,46] the escape over a potential barrier of height ΔE is retarded by a Boltzmann factor $\exp(\Delta E/k_B T)$. For the diffusive motion of P_i in the ion potential (picosecond timescale), the above values for the barrier heights would lead to escape times on the order of 10^9 s (HPO_4^{2-}) and 10^2 s ($H_2PO_4^-$). In this scenario, HPO_4^{2-} would remain trapped in the potential well of the Ca^{2+} ion. Only its protonation would allow the phosphate to escape the cation on the biological timescale.

Interactions With Actin

After liberation from the ion, the simulation path allows for the release of the phosphate without significant disturbance to the structure of actin (Fig. 5). The Ca^{2+}-ATP-actin system had been simulated earlier for a total simulation
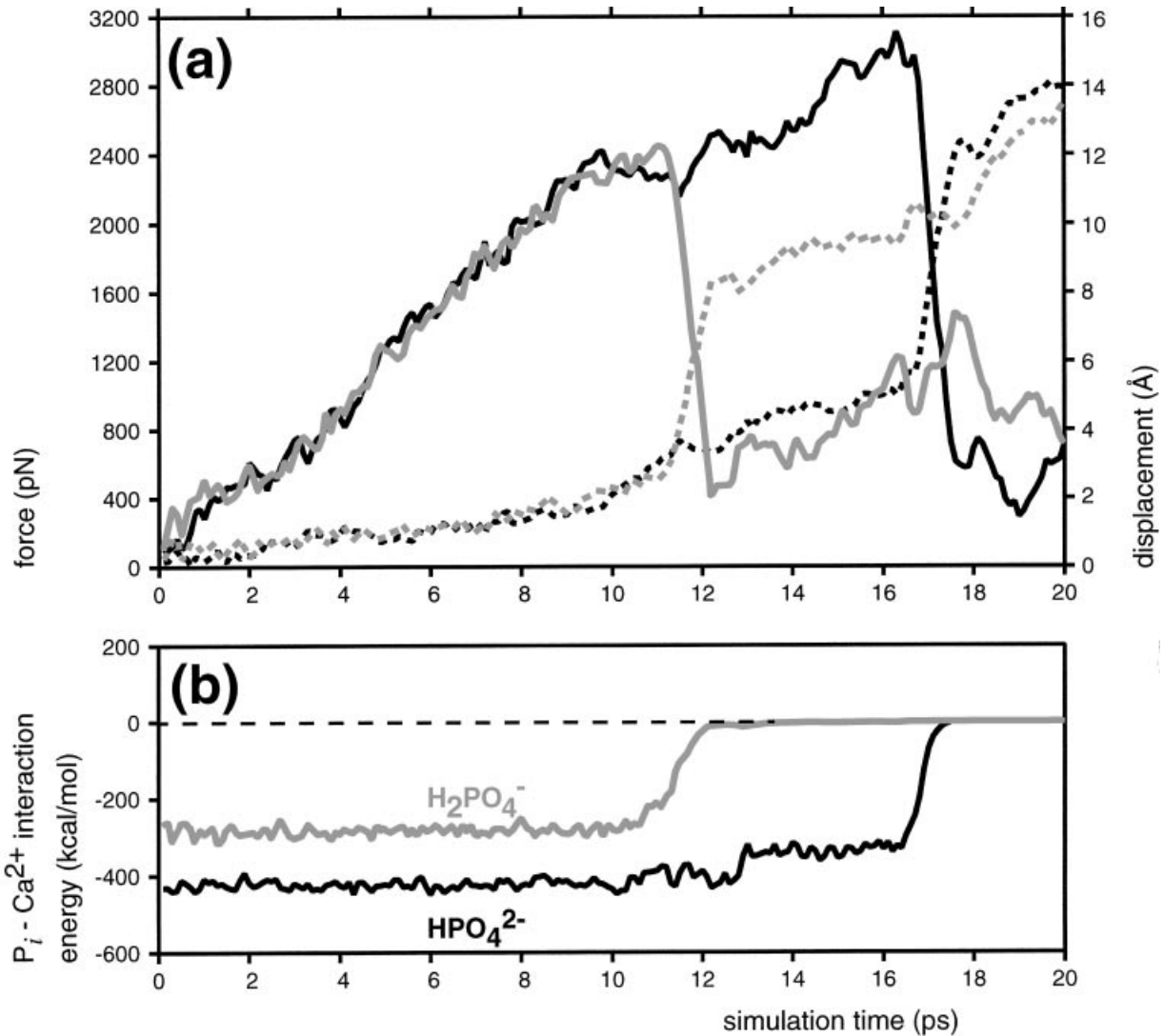
Fig. 4.   Characteristics describing the release of P$_i$ in the presence of Ca^{2+}. **a:** Force exerted on P$_i$ by the restraint (solid line) and displacement of P$_i$ from its position after heat-up/equilibration (dotted line) for H$_2$PO$_4^-$ (grey) and HPO$_4^{2-}$ (black); **b:** the corresponding electrostatic interaction energies between P$_i$ and the Ca^{2+} ion. The simulation time excludes the time of the initial heat-up/equilibration (10 ps).

time of 500 ps.[15] This simulation provided a control that allowed us to assess the effect of P$_i$ separation on the stability and dynamics of the protein. As an example, we compare the simulation of HPO$_4^{2-}$ release in the presence of Ca^{2+} to the control simulation; other simulations exhibited similar behavior (data not shown). The changes in the protein structure were monitored through the root mean square (rms) deviation of the α-carbon atoms from the initial structure (Fig. 5) and through the temperature increase of the system. The rms deviation of the structure during phosphate dissociation exceeded the rms deviation in the control simulation (1.5 Å) only slightly, i.e., by about 0.3 Å (Fig. 5a). SMD simulations of retinal extraction from bacteriorhodopsin resulted in a temperature increase of 40 K caused by irreversible work performed on the system during separation of the ligand retinal.[19] In comparison,

the temperature increased only moderately by 10–15 K in the simulations described in this work (data not shown).

In addition to the simulations in the presence of Ca^{2+}, we performed simulations of P$_i$ release from divalent cation-free actin. These simulations reveal important interactions of P$_i$ with amino acid residues in the putative separation pathway that would otherwise be obscured by the pronounced jump in the displacement due to the interaction with the ion (Fig. 4a). The improved sampling of interactions with actin at intermediate P$_i$ displacements also allowed us to distinguish between specific interactions with protein side chains, and nonspecific, velocity-dependent interactions in the separation channel due to friction. To this end, we extracted the phosphate at different dissociation velocities. The accuracy of the simulation of P$_i$ motion after its liberation from the ion relies on two
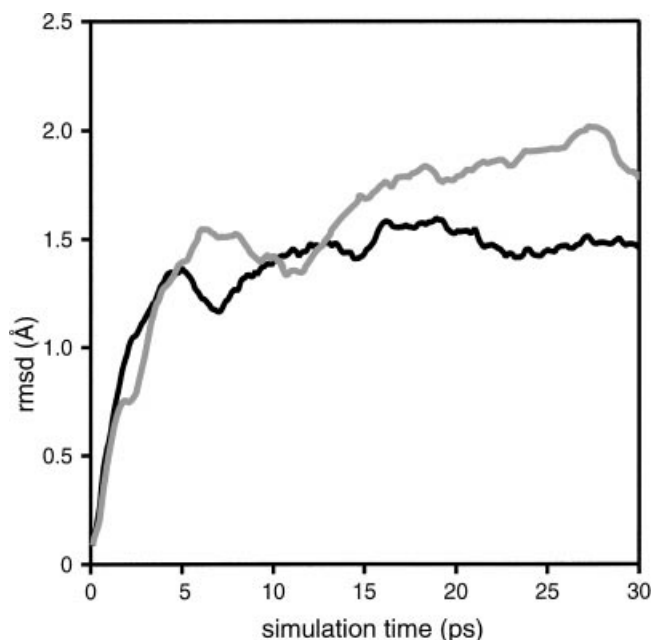
Fig. 5. RMS deviation of α-carbons from the initial structure. The values shown correspond to the simulation of HPO_4^{2-} release from Ca^{2+}-actin (grey) and to the control simulation (black) reported elsewhere.[15]

assumptions: (1) the slow escape of P_i over the ion potential barrier (see above) is stochastic and does not require a conformational change of the protein; (2) the subsequent P_i release is sufficiently fast, as suggested by the overall kinetics of ligand-receptor binding (see above), such that conformational changes orthogonal to the pull direction are sampled on the short timescales accessible to SMD.

Does P_i follow a unique separation path in the absence of the divalent cation? Figure 6 demonstrates that considerable variability arises in the forces corresponding to small displacements from the initial position of P_i. An inspection of the "animated" dynamics of P_i extraction with the molecular graphic program VMD[47] revealed that the pronounced peaks in the measured forces (Fig. 6) are caused by the breaking of hydrogen bonds when P_i is liberated from its binding pocket. In a given realization of P_i dissociation, the strength of the hydrogen bonds with coordinating groups is sensitive to the particular position of the phosphate relative to neighboring residues. $H_2PO_4^-$ was found to interact strongly with actin's Ser14, Gln137, and Val159. An initial contact of one of the hydrogens with a nearby oxygen of the ADP β-phosphate was also observed in two cases (simulations of length 128 and 256 ps). In comparison, singly protonated P_i formed strong bonds mainly with the side chain of actin's Ser14 and with bridging water molecules that coordinated both HPO_4^{2-} and the ADP β-phosphate (see Fig. 2b).

The animation of the simulation trajectories identified a total of ten residues that made contact with the phosphate along its separation path. The observed number of interactions with P_i in each of the two sets of trajectories of like P_i

protonation states are given in Figure 7. Two snapshots (Fig. 8) exemplify the coordination of $H_2PO_4^-$ by Ser14, Gln137, and the ADP β-phosphate, and of HPO_4^{2-} by His73 and Arg177. Initially P_i participates in interactions with the side chains of Ser14, Gln137, and Val159, with the main chains of glycines 13, 74, and 158 and, transiently, with Ile71. These initial contacts break in the course of the simulations and, in certain cases, new hydrogen bonds with His73, His161, and Arg177 are formed at a later stage of the dissociation process (Fig. 7). The contact frequencies reveal that the length of the positively charged Arg177 side chain allows this residue to interact with the phosphate for nearly the full range of P_i displacement.

The protonation of P_i altered the propensity of the phosphate to form a contact with the side chain of methylated His73. In the simulations involving HPO_4^{2-}, His73$^+$ formed hydrogen bonds with P_i (Fig. 7b). The contact with $H_2PO_4^-$ required a reorientation of His73 (Fig. 8b) relative to its position in the crystal structure, where the imidazole points to the side opposite to the phosphate (Fig. 1). In the simulations involving $H_2PO_4^-$, methylated His73$^+$ did not coordinate the phosphate (Fig. 7a). The protonation of P_i also weakened the initial interactions with Gly13 and Ser14 (Fig. 7). The effect of the protonation on residues other than Gly13, Ser14, and His73 appears to be less significant.

Solvation Effects

Solvation is likely to influence the forces measured in SMD simulations. In simulations of the streptavidin-biotin complex,[17] the binding pocket was exposed to the solvent. This allowed water molecules to enter the binding pocket and participate in breaking hydrogen bond networks between the ligand and the protein during the dissociation. Grubmüller et al.[17] observed a decreasing force with decreasing dissociation velocity v, which was attributed to a frictional contribution that depends linearly on v. In this work, P_i is coordinated by three or fewer actin residues (Fig. 7) once the displacement of the phosphate from its position after cleavage exceeded 5 Å. Water molecules in the solvated back-door channel, which compete with actin's residues for hydrogen bonds, provide the remaining coordination of P_i. We investigated whether or not the reduced number of interactions with the protein gave rise to frictional contributions to the dissociation force, which decrease with smaller dissociation velocity v.

Table I presents the averages and standard deviations of the exerted force computed from the trajectories of divalent cation-free actin for displacements less than 5 Å and for displacements greater than 5 Å. The average forces, for displacements less than 5 Å, exhibited considerable variations (400–930 pN). These force variations are due to the variability of specific interactions with actin residues in the initial phase of P_i release (see above). For displacements greater than 5 Å, the average forces generally decreased with smaller dissociation velocities to values as low as 400 pN (for $H_2PO_4^-$) and 510 pN (for HPO_4^{2-}). This trend was generally observed for both phosphate protonation states, albeit HPO_4^{2-} exhibited higher extraction
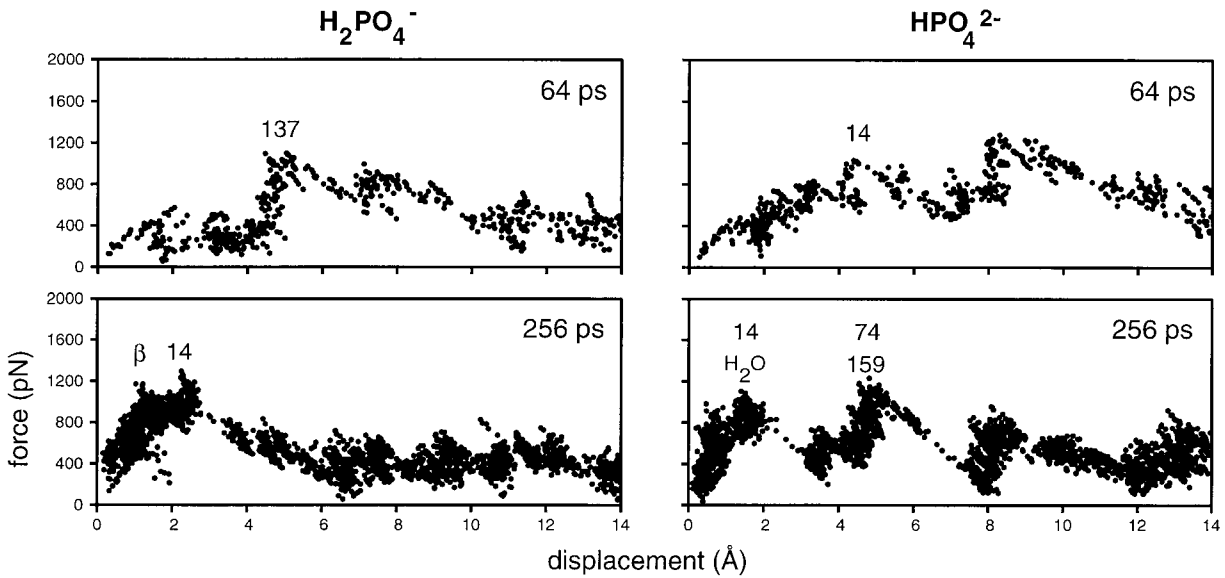
Fig. 6. Forces exerted on P$_i$ as a function of its displacement in selected simulations of divalent cation-free actin. The breaking of contacts with groups in the P$_i$ binding site, corresponding to peaks in the measured forces, are marked as follows: "β" indicates the breaking of a direct hydrogen bond between P$_i$ and a β-phosphate oxygen of ADP; "H$_2$O" denotes the breaking of a water bridge between P$_i$ and a β-phosphate oxygen; the breaking of contacts with amino acids are indicated by the respective residue number. The simulation lengths correspond to the times of Table I.
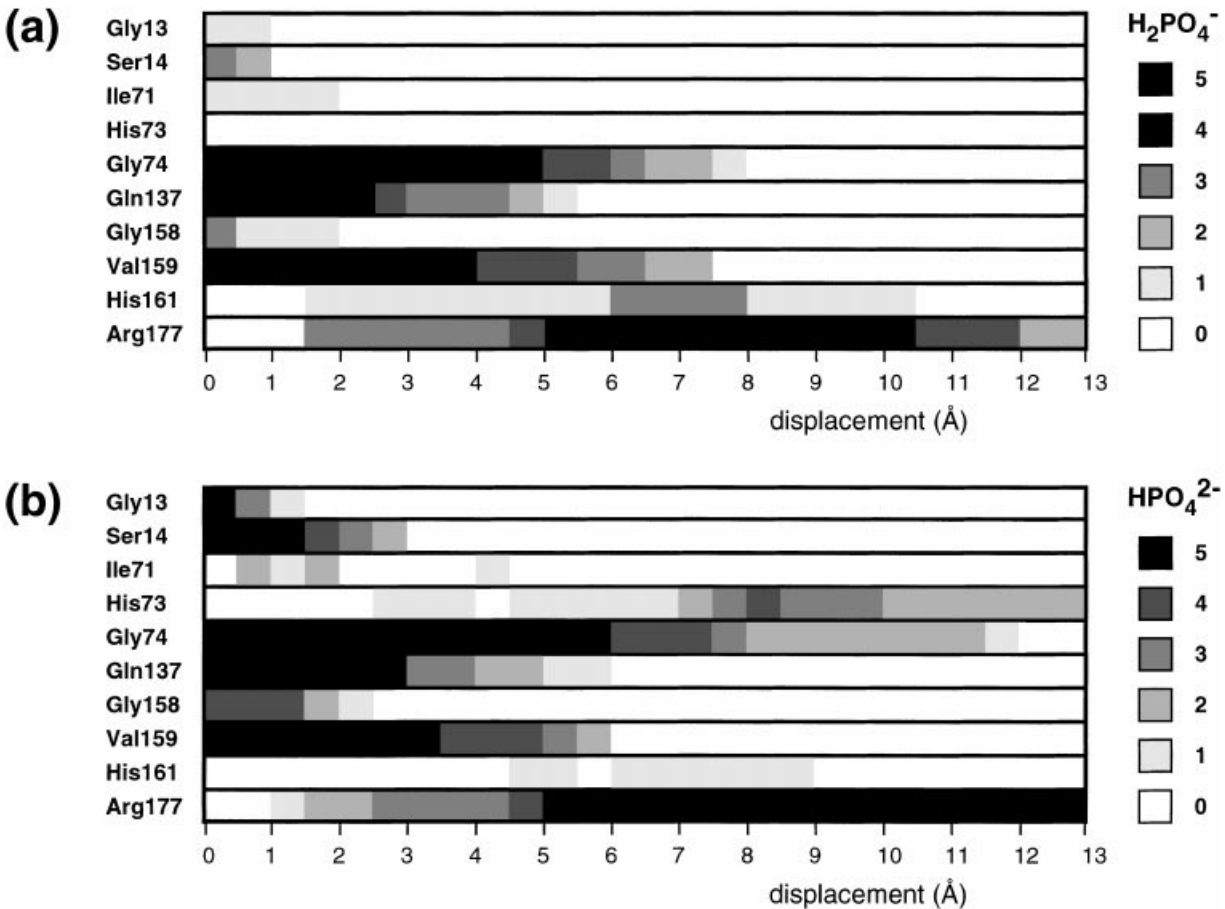
Fig. 7. Number of P$_i$ contacts exhibited by residues of divalent cation-free actin as a function of displacement. Displacement-dependent hydrogen bonds with the side chain (Gly: main chain) of P$_i$-coordinating residues were identified using VMD.[47] The number of contacts at comparable displacements was determined from five simulations of like P$_i$ protonation state (see Table I). a: Number of contacts in five simulations involving H$_2$PO$_4^-$; b: number of contacts in five simulations involving HPO$_4^{2-}$.
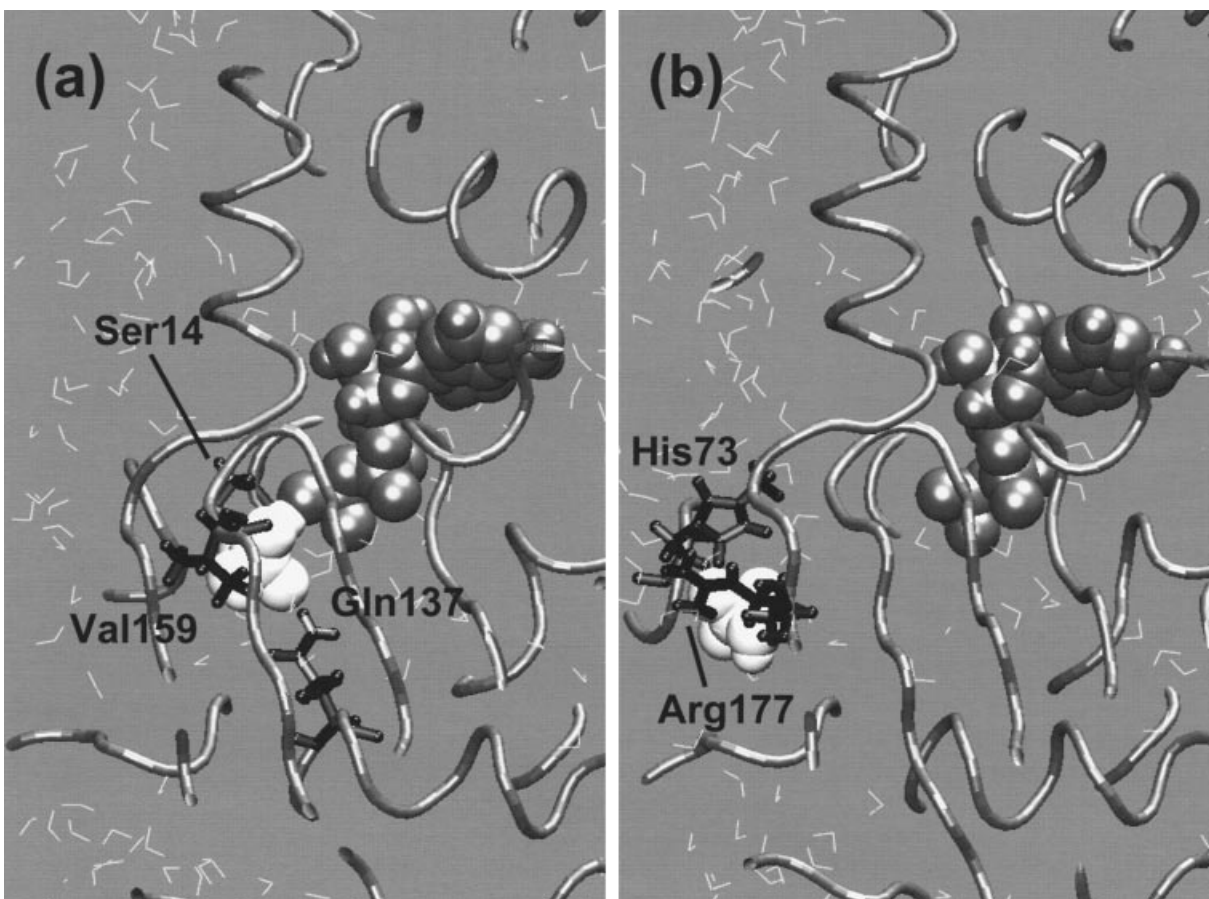
Fig. 8.   Contacts of P_i with actin residues and with ADP. ADP (grey), Ca^{2+} (black), and the dissociated P_i (white) are shown in van-der-Waals sphere representation. The protein backbone is shown in tube representation. The orientation of the protein corresponds to the view in Figure 3. **a:** Dissociation of $H_2PO_4^-$ from divalent-cation-free actin, after equilibra-tion. Ser14, Val159 and Gln137 are shown in black licorice style. **b:** Dissociation of HPO_4^{2-} from divalent-cation-free actin, after 8 ps P_i dissociation (total simulation length 32 ps). His73 and Arg177 are shown in black licorice style. The figure was generated using the molecular graphics program VMD.[47]

TABLE I. P_i Extraction From Divalent-Cation-Free Actin[†]

Simulation time (ps)		Simulation time (ps)				
		16	32	64	128	256
$H_2PO_4^-$						
Force (pN)	<5 Å	530 ± 220	410 ± 280	400 ± 220	530 ± 220	740 ± 210
Ave. $\pm$ SD	>5 Å	640 ± 190	570 ± 230	550 ± 220	470 ± 150	400 ± 120
HPO_4^{2-}						
Force (pN)	<5 Å	670 ± 250	680 ± 310	520 ± 200	930 ± 460	640 ± 230
Ave. $\pm$ SD	>5 Å	840 ± 180	$1,050 \pm 200$	770 ± 210	660 ± 150	510 ± 190

[†]Shown are the extraction forces observed for displacements less than 5 Å and for displacements greater than 5 Å. For each simulation (see Methods) the average and standard deviation (SD) of the forces were computed from the trajectories, excluding the initial heat-up/equilibration.

forces than $H_2PO_4^-$ at comparable dissociation velocities. Hence, after liberation of P_i from its binding pocket, the forces exerted on the phosphate follow a force-velocity relationship similar to the one described in Grubmüller et al.[17] (Table I).

We note that the 32 ps simulation involving HPO_4^{2-} provided the sole exception to the observed decrease of the average force with smaller dissociation velocities. The high adhesion force of 1,050 pN in this simulation was caused by a stable attachment of the His73 side chain to the dissociating P_i for displacements greater than 4.5 Å, which induced a strain in the main chain of the protein (Fig. 8b).

To consider the effect of water mobility on a ligand that undergoes uniform motion in a narrow, water-filled channel such as present in actin, we estimate the relaxation time of water molecules in the channel. It is assumed that

the motion of water molecules is governed by one-dimensional diffusion. The diffusion coefficient along the channel axis, D_z, is then characterized by

$$\langle [z(\tau + t) - z(\tau)]^2 \rangle = 2D_z t, \tag{2}$$

where $\langle \cdots \rangle$ denotes an average over time origins τ and over the water molecules in the channel, $z(t)$ is the position of a water molecule at the offset time t. We can approximate the width of a layer of water molecules, d_0, by the size of a single water molecule, $d_0 = 3.2$ Å. The time t_0 required to exchange, by diffusion, a water molecule in the layer is then

$$t_0 = \frac{d_0^2}{2D_z}. \tag{3}$$

The three-dimensional self-diffusion coefficient of bulk water at 300 K is $D = 0.23$ Å^2/ps.[48] In the case of one-dimensional diffusion in narrow channels of radius 2–3 Å, the coefficient is reduced to a value $D_z = 0.06$ Å^2/ps,[49,50] resulting in a water exchange time of $t_0 = 85$ ps. This value is only slightly lower than the shortest experimentally observed exchange times of water molecules in the hydration shell of solvated ions, which can be as low as 300 ps.[51]

With the help of Eq. 3, we can compute a critical pull velocity v_{crit}, at which the time required to traverse the distance d_0, $t = d_0/v_{crit}$, equals the diffusive water exchange time

$$v_{crit} = \frac{2D_z}{d_0}. \tag{4}$$

The values of D_z and d_0 assumed above yield a critical velocity $v_{crit} = 0.0375$ Å/ps. For dissociation velocities $v \gg v_{crit}$, the slow diffusion of water molecules in the system can not fill the space freed by fast displacement of the ligand, and the separation of the ligand proceeds as the hydrogen-bond network of the surrounding, relatively immobile matrix of water molecules is fractured, forming empty cavities in the wake of the ligand. For dissociation velocities $v \gg v_{crit}$, the diffusing water molecules form a lubricating cloud of transient hydrogen bonds. The dissociation velocities in this work, which range from 0.0625 Å/ps ($< v_{crit}$) to 1 Å/ps ($> v_{crit}$), suggest that the decreasing forces observed in slow dissociation simulations are likely due to an increased lubrication effect as the water molecules gain mobility relative to the displaced phosphate.

DISCUSSION

Steered molecular dynamics provides the possibility to induce relatively large conformational changes in ligand-receptor complexes on the time scales accessible to MD simulations. The simulations furnish a qualitative picture of non-covalent dissociation processes. In this work, we have applied SMD and convential MD to corroborate a model of P$_i$ release from actin through a separation path that was found earlier[15] to provide solvent access to actin's

enzymatic site. The forces required for extraction of (doubly protonated) P$_i$ after liberation from its binding pocket in divalent cation-free actin are due to friction and do not indicate any significant potential barriers. The separation of P$_i$ proceeds smoothly and the forces exerted on the phosphate settle at low values near 400 pN for low dissociation velocities v (Table I).

The simulations provide a clear prediction of the time-limiting step of P$_i$ release from actin, namely, the breaking of strong electrostatic interactions of P$_i$ with the divalent cation that is associated with the nucleotide. The results suggest also that protonation of P$_i$ promotes dissociation from the cation: titration of HPO$_4^{2-}$ to H$_2$PO$_4^-$ significantly lowers the cation-related electrostatic barrier, which the phosphate needs to overcome. Assuming a dielectric constant $\epsilon = 15$ of the protein/solvent environment in actin's catalytic site, the estimated electrostatic interaction energies with Ca^{2+} are 29 and 19 kcal/mol for HPO$_4^{2-}$ and H$_2$PO$_4^-$, respectively. Protonation of P$_i$ also lowers the adhesion to actin residues that line the separation channel, notably, His73.

The simulations in this work were carried out based on the Ca^{2+}-actin structure. In the cell, this ion is most likely replaced by Mg^{2+} (reviewed in Estes et al.[14]). Experiments suggest that Mg^{2+} binding induces a conformational change in the protein,[52] but the structure of Mg^{2+}-actin is not known in atomic detail. The experimental literature demonstrates considerable differences between Ca^{2+}- and Mg^{2+}-actin in terms of ATP hydrolysis and polymerization behavior.[6,14,53] Due to a smaller van-der-Waals radius of Mg^{2+} (0.65 Å compared to 0.99 Å of Ca^{2+}),[39] the electrostatic metal-P$_i$ interactions should be considerably stronger for Mg^{2+}. Consistent with this idea, ion-coordinating ligands appear to be held more tightly and the dissociation of the ion from the high-affinity binding site on Mg^{2+}-actin is slower.[14] By analogy, one would therefore expect a slower P$_i$ release from Mg^{2+}-actin relative to Ca^{2+}. However, P$_i$ release as well as ATP hydrolysis are actually promoted by Mg^{2+} relative to Ca^{2+}.[44,54] Thus, the differences in the behavior of Mg^{2+}- and Ca^{2+}-actin cannot be explained by the ionic radius alone. The release of P$_i$ could be enhanced by a conformational change in Mg^{2+}-actin that lowers the height of the electrostatic barrier or stabilizes the protonated H$_2$PO$_4^-$.

Actin hydrolyzes ATP during the G-F transformation. The aggregation into filaments may induce a change of actin's conformation.[24,55] Are the simulations based on a G-actin crystal structure relevant for P$_i$ release from F-actin? The effect of phalloidin-binding to F-actin suggests that a possible conformational change associated with the G-F transformation does not alter the described release of the phosphate: Kinetic measurements indicate a phalloidin-induced delay in P$_i$ release.[25] This delay is probably due to steric hindrance, since the exit of the phosphate separation pathway (Wriggers and Schulten[15]; this work) forms part of actin's phalloidin binding face.[24] In the absence of phalloidin, F-actin's phosphate separation pathway appears viable. Three-dimensional reconstructions of electron micrographs reveal a conformational

difference between ADP-P$_i$ filaments and ADP filaments, and show that the crystal structure used in this work fits very well the F-actin data in the presence of ADP-P$_i$.[56]

In the absence of divalent cation, the simulations reveal a propensity of His73$^+$ to form a salt bridge with HPO$_4^{2-}$, but not with H$_2$PO$_4^-$. Interactions with H$_2$PO$_4^-$ occurred at displacements as small as 2.5 Å (Fig. 7b), which is close to the thermally accessible range of conformational fluctuations (1.5 Å[15]) if HPO$_4^{2-}$ were still bound to the Ca^{2+} ion. Although a salt bridge with HPO$_4^{2-}$ was not observed in the presence of the ion, the His73$^+$ side chain came within 5 Å of the nearest phosphate oxygen, a distance readily bridged by a water molecule. By analogy to pKa shifts observed in a His-Asp salt bridge in T4 lysozyme,[57] one can estimate that a direct salt bridge between His73$^+$ and HPO$_4^{2-}$ would lower the pKa of H$_2$PO$_4^-$ by 3–4 units relative to its value in solution (pKa = 7.21), i.e., His73$^+$ would stabilize singly protonated HPO$_4^{2-}$. A water bridge between His73 and P$_i$ would also stabilize HPO$_4^{2-}$, albeit to a lesser degree. The methyl group, which in most actin species is added to His73 by a posttranslational modification at the expense of metabolic energy, would promote the ability of His73 to assume the charged, P$_i$-stabilizing state.

The importance of the charge at the position of residue 73 is confirmed by His/Tyr mutants that exhibit a slightly greater critical concentration for polymerization.[27] A more drastic effect was recently described for a His73/Ala mutant: ATP turn-over (hydrolysis and/or Pi-release) relative to net-polymerization was faster than observed for the wild type (T. Nyman and R. Karlsson, personal communication). The difference from wild type actin could be explained by an increased subunit exchange at His73/Ala mutant filament ends leading to the hydrolysis of more than one ATP per actin subunit incorporated. This interpretation is consistent with our model: The stabilization of singly protonated P$_i$ by His73 would delay its protonation and, thus, its release from actin. Retention of P$_i$ stabilizes, in turn, the elongating filaments in the cytoskeleton.

In addition to His73, our results also suggest a stabilizing function for Arg177. The flexibility of its side chain allowed Arg177 to coordinate P$_i$ along the separation pathway, starting at displacements as low as 1 Å and ending at the exit of P$_i$ (Fig. 7). Arg177 may act as a shuttle that mediates the transport of P$_i$ to a second binding site on the surface of the protein. The presence of a second binding site for P$_i$ is supported by bimodal effects of P$_i$-like BeF$_n$ on the fluorescence of F-PIA-ADP actin.[23] As described by Allen et al.,[23] the two P$_i$ binding sites would be sequentially occupied during phosphate release.

New kinetic and mutagenesis experiments will further elucidate the mechanism of actin's phosphate release. In particular, we expect that the temperature-dependent P$_i$ dissociation rate follows the Arrhenius law,[46] which would confirm a single rate limiting step (the liberation from the divalent cation) and reveal the activation energy. Mutations of Val159 or Gly74 that positively charge the residue should decrease the rate of P$_i$ release. A mutation of Val159 to Asn uncouples P$_i$ release from a conformational change observed in yeast actin[56] and confirms a critical role of this residue in the time-dependent assembly and disassembly of the cytoskeleton.

REFERENCES

1. Small JV. Microfilament-based motility in non-muscle cells. Curr Opin Cell Biol 1989;1:75–79.
2. Theriot JA, Mitchison TJ, Tilney LG, Portnoi DA. The rate of actin-based motility of intracellular *Listeria monocytogenes* equals the rate of actin polymerization. Nature 1992;357:257–260.
3. Devreotes PN, Zigmond SH. Chemotaxis in eukaryotic cells: a focus on leukocytes and *Dictyostelium.* Ann Rev Cell Biol 1988;4: 649–686.
4. Carlier M-F. Role of nucleotide hydrolysis in the dynamics of actin filaments and microtubules. Int Rev Cytol 1989;115:139–170.
5. Melki R, Fievez S, Carlier M-F. Continuous monitoring of P$_i$ release following nucleotide hydrolysis in actin or tubulin using 2-amino-6-mercapto-7-methylpurine ribonucleoside and purine-nucleoside phosphorylase as an enzyme-linked assay. Biochemistry 1996;35:12038–12045.
6. Carlier M-F. Actin: Protein structure and filament dynamics. J Biol Chem 1991;266:1–4.
7. Pollard TD, Goldberg I, Schwarz WH. Nucleotide exchange, structure, and mechanical properties of filaments assembled from ATP-actin and ADP-actin. J Biol Chem 1992;267:20339–20345.
8. Isambert H, Venier P, Maggs AC, Fattoum A, Kassab R, Pantaloni D, Carlier MF. Flexibility of actin filaments derived from thermal fluctuations. J Biol Chem 1995;270:11437–11444.
9. Carlier M-F, Pantaloni D. Binding of phosphate to F-ADP-actin and role of F-ADP-P$_i$-actin in ATP-actin polymerization. J Biol Chem 1988;263:817–825.
10. Kabsch W, Mannherz HG, Suck D, Pai EF, Holmes KC. Atomic structure of the actin:DNase I complex. Nature 1990;347:37–44.
11. Holmes KC, Kabsch W. Muscle proteins: actin. Curr Opinion Struct Biol 1991;1:270–280.
12. McLaughlin PJ, Gooch JT, Mannherz H-G, Weeds AG. Structure of gelsolin segment 1-actin complex and the mechanism of filament severing. Nature 1993;364:685–692.
13. Fothergill M, Goodman MF, Petruska J, Warshel A. Structure-energy analysis of the role of metal ions in phosphodiester bond hydrolysis by DNA polymerase I. J Am Chem Soc 1995;117:11619–11627.
14. Estes JE, Selden LA, Kinosian HJ, Gershman LC. Tightly-bound divalent cation of actin. J Muscle Res Cell Mot 1992;13:272–284.
15. Wriggers W, Schulten K. Stability and dynamics of G-actin: Back door water diffusion and behavior of a subdomain 3/4 loop. Biophys J 1997;73:624–639.
16. Allen MP, Tildesley DJ. Computer simulation of liquids. New York: Oxford University Press; 1987.
17. Grubmüller H, Heymann B, Tavan P. Ligand binding and molecular mechanics calculation of the streptavidin-biotin rupture force. Science 1996;271:997–999.
18. Izrailev S, Stepaniants S, Balsera M, Oono Y, Schulten K. Molecular dynamics study of unbinding of the avidin-biotin complex. Biophys J 1997;72:1568–1581.
19. Isralewitz B, Izrailev S, Schulten K. Binding pathway of retinal to bacterio-opsin: A prediction by molecular dynamics simulations. Biophys J 1997;73:2972–2979.
20. Izrailev S, Stepaniants S, Isralewitz B, Kosztin D, Lu H, Molnar F, Wriggers W, Schulten K. Steered molecular dynamics. In: Deuflhard P, Hermans J, Leimkuhler B. In: Mark AE, Reich S, Skeel RD, editors. Computational molecular dynamics: challenges, methods, ideas. Berlin/Heidelberg: Springer-Verlag, 1999.
21. Knowles JR. Enzyme-catalyzed phosphoryl transfer reactions. Ann Rev Biochem 1980;49:877–919.
22. Fersht A. Enzyme structure and mechanism. New York: W.H. Freeman and Co.; 1985.

23. Allen PG, Laham LE, Way M, Janmey PA. Binding of phosphate, aluminum fluoride, or beryllium fluoride to F-actin inhibits severing by gelsolin. J Biol Chem 1996;271:4665–4670.

24. Lorenz M, Popp D, Holmes KC. Refinement of the F-actin model against X-ray fiber diffraction data by the use of a directed mutation algorithm. J Mol Biol 1993;234:826–836.

25. Dancker P, Hess L. Phalloidin reduces the release of inorganic phosphate during actin polymerization. Biochim Biophys Acta 1990;1035:197–200.

26. Sussman DJ, Sellers JR, Flicker P, Lai EY, Cannon LE, Szent-Györgyi AG, Fulton C. Actin of *Naegleria gruberi.* J Biol Chem 1984;259:7349–7354.

27. Solomon LR, Rubenstein PA. Studies on the role of actin's N-methylhistidine using oligodeoxynucleotide-directed site-specific mutagenesis. J Biol Chem 1987;262:11382–11388.

28. Dawson RMC, Elliott DC, Elliott WH, Jones KM. Data for biochemical research. Oxford: Clarendon Press; 1986.

29. Brünger AT. X-PLOR, Version 3.1: a system for X-ray crystallography and NMR. New Haven: The Howard Hughes Medical Institute and Department of Molecular Biophysics and Biochemistry, Yale University; 1992.

30. Brooks BR, Bruccoleri RE, Olafson BD, States DJ, Swaminathan S, Karplus M. CHARMM: A program for macromolecular energy, minimization, and dynamics calculations. J Comp Chem 1983;4: 187–217.

31. Zhang L, Hermans J. Hydrophilicity of cavities in proteins. Proteins: Struct Funct Genet 1996;24:433–438.

32. Wriggers Willy. Structure, Function, and Dynamics of Cell Motility Proteins. PhD thesis, University of Illinois at Urbana-Champaign; 1998.

33. Jorgensen WL, Chandrasekhar J, Madura JD, Impey RW, Klein ML. Comparison of simple potential functions for simulating liquid water. J Chem Phys 1983;79:926–935.

34. Wriggers W, Mehler E, Pitici F, Weinstein H, Schulten K. Structure and dynamics of calmodulin in solution. Biophys J 1998;74: 1622–1639.

35. Frisch MJ, Trucks GW, Schlegel HB, Gill PMW, Johnson BG, Robb MA, Cheeseman JR, Keith T, Petersson GA, Montgomery JA, Raghavachari K, Al-Laham MA, Zakrzewski VG, Ortiz JV, Foresman JB, Peng CY, Ayala PY, Chen W, Wong MW, Andres JL, Replogle ES, Gomperts R, Martin RL, Fox DJ, Binkley JS, Defrees DJ, Baker J, Stewart JP, Head-Gordon M, Gonzalez C, Pople JA. Gaussian 94, Revision B.3. Pittsburgh, PA: Gaussian Inc.; 1995.

36. Evans E, Ritchie K. Dynamic strength of molecular adhesion bonds. Biophys J 1997;72:1541–1555.

37. Flaherty KM, Wilbanks SM, DeLuca-Flaherty C, McKay DB. Structural basis of the 70-kilodalton heat shock cognate protein ATP hydrolytic activity. J Biol Chem 1994;269:12899–12907.

38. Flaherty KM, McKay DB, Kabsch W, Holmes KC. Similarity of the three-dimensional structures of actin and the ATPase fragment of a 70-kDa heat shock cognate protein. Proc Natl Acad Sci USA 1991;88:5041–5045.

39. Israelachvili JN. Intermolecular and surface forces. London: Academic Press; 1992.

40. King G, Lee FS, Warshel A. Microscopic simulations of macroscopic dielectric constants of proteins. J Chem Phys 1991;95:4366–4377.

41. Smith PE, Brunne RM, Mark AE, van Gunsteren WF. Dielectric properties of trypsin inhibitor and lysozyme calculated from molecular dynamics simulations. J Phys Chem 1993;97:2009–2014.

42. Elber R, Karplus M. Enhanced sampling in molecular dynamics: Use of the time-dependent Hartree approximation for a simulation of carbon monoxide diffusion through myoglobin. J Am Chem Soc 1990;112:9161–9175.

43. Creighton TE. Proteins, 2nd ed. New York: W. H. Freeman and Company; 1993.

44. Carlier M-F, Pantaloni D. Direct evidence for ADP-P$_f$-F-actin as the major intermediate in ATP-actin polymerization. Rate of dissociation of P$_i$ from actin filaments. Biochemistry 1986;25:7789–7792.

45. Gardiner CW. Handbook of stochastic methods for physics, chemistry, and the natural sciences. New York: Springer-Verlag; 1985.

46. Cantor CR, Schimmel PR. Biophysical chemistry, volume III. New York: W.H. Freeman and Company; 1980.

47. Humphrey WF, Dalke A, Schulten K. VMD: visual molecular dynamics. J Mol Graphics 1996;14:33–38.

48. Eisenberg D, Kauzmann W. The structure and properties of water. Oxford: Oxford University Press; 1969.

49. Breed J, Sankararamakrishnan R, Kerr ID, Sansom MSP. Molecular dynamics simulations of water within models of ion channels. Biophys J 1996;70:1643–1661.

50. Sansom MSP, Kerr ID, Breed J, Sankararamakrishnan R. Water in channel-like cavities: Structure and dynamics. Biophys J 1996;70:693–702.

51. Cotton FA, Wilkinson G. Advanced inorganic chemistry. New York: Interscience Publishers; 1966.

52. Strzelecka-Golaszewska H, Wozniak A, Hult T, Lindberg U. Effects of the type of divalent cation, Ca^{2+} or Mg^{2+}, bound at the high-affinity site and of the ionic composition of the solution on the structure of F-actin. Biochem J 1996;316:713–721.

53. Kinosian HJ, Selden LA, Estes JE, Gershman LC. Nucleotide binding to actin. J Biol Chem 1993;268:8683–8691.

54. Selden LA, Kinosian HJ, Estes JE, Gershman LC. Simultaneous and continuous measurements of actin polymerization and phosphate release: Watching the phosphate clock. Biophys J 1998;74: A48 (abstract M-POS23).

55. Tirion MM, ben-Avraham D, Lorenz M, Holmes KC. Normal modes as refinement parameters for the F-actin model. Biophys J 1995;68:5–12.

56. Belmont LD, Orlova A, Drubin DG, Egelman EH. A change in actin conformation associated with filament instability after P$_i$ release. Proc Natl Acad Sci USA 1999;96:29–34.

57. Anderson DE, Becktel Wayne J, Dahlquist FW. pH-Induced denaturation of proteins: a single saltbridge contributes 3–5 kcal/mol to the free energy of folding of T4 lysozyme. Biochemistry 1990;29:2403–2408.